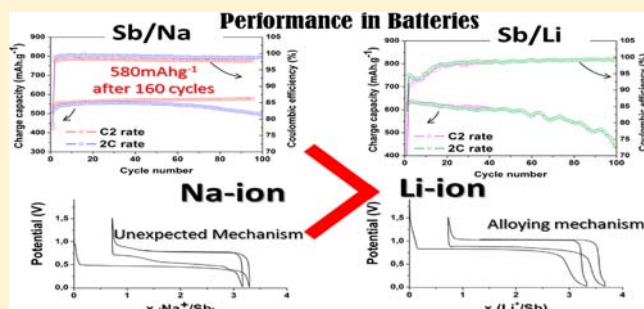


Better Cycling Performances of Bulk Sb in Na-Ion Batteries Compared to Li-Ion Systems: An Unexpected Electrochemical Mechanism

Ali Darwiche, Cyril Marino, Moulay T. Sougrati, Bernard Fraisse, Lorenzo Stievano, and Laure Monconduit*

Institut Charles Gerhardt UMR CNRS 5253, ALISTORE European Research Institute (3104 CNRS) – AIME, Université Montpellier 2, CC1502, place E. Bataillon, 34095 Montpellier cedex 5, France

ABSTRACT: Pure micrometric antimony can be successfully used as negative electrode material in Na-ion batteries, sustaining a capacity close to 600 mAh g^{-1} at a high rate with a Coulombic efficiency of 99 over 160 cycles, an extremely high capacity compared to any other compound tested against both Li and Na. The reaction mechanism with Na does not simply go through the alloying mechanism observed for Li where the intermediate species are those expected from the phase diagram. In the case of Na, the intermediate phases are mostly amorphous and could not be precisely identified. Surprisingly, we evidenced that a competition takes place at the end of the discharge of the Sb/Na cell between the formation of the hexagonal and the cubic polymorphs of Na_3Sb , the last being described in the literature as unstable at atmospheric pressure and only synthesized under high pressure (1–9 GPa). In addition, fluoroethylene carbonate added to the electrolyte combined with an appropriate electrode formulation based on carboxymethyl cellulose, carbon black, and vapor ground carbon fibers seems to be determinant in the excellent performances of this material.



INTRODUCTION

In recent years, the use of Li-ion batteries in portable devices and electric vehicles has strongly expanded. However, the Earth's limitation of lithium-rich resources, due to the increasing use of Li-ion batteries for consumer applications and for electric vehicles, is expected to strongly influence the price and the availability of lithium in the long term.¹ Even though lithium starts being recycled, sodium-ion batteries are a possible near-term substitute for large-scale systems (e.g., grid storage) because of the greater abundance and lower cost of sodium-containing precursors.² Unlike Li, Na is one of the most abundant elements on the Earth's crust, and its production is relatively simple and clean. For this reason, batteries employing Na instead of Li ions are globally more environmentally benign. After a period of active research on Na-based batteries in the past decades,³ Na-ion batteries have recently regained interest. Even though recent research has been mainly centered on positive electrode materials,^{4–6} several works have also been devoted to the negative ones, mainly carbon-based composites. While graphite has poor Na^+ insertion properties, hard carbon can sustain a capacity as large as 300 mAh g^{-1} thanks to pseudocapacitive Na^+ surface adsorption.^{7–9} One of the main limitations to the widespread use of Na-ion batteries could be the larger ionic radius of Na^+ compared to Li^+ . In fact, even though it has been demonstrated that in some specific host structures such as Nasicon Na^+ ion diffusion is predicted to be faster than that of Li^+ ,¹⁰ the larger

ionic radius presents a steric limitation in numerous host structures, leading to a higher volume expansion upon cycling. If on the one hand this feature causes limitations for insertion materials, i.e., most cathode and numerous anode materials, on the other hand it is expected to have a lower impact on conversion or alloying/dealloying processes which are common to many anode materials.¹¹ In fact, the higher value of the Na^+/Na potential compared to Li^+/Li is expected to reduce electrolyte degradation at the surface of the electrode material. The latter is a very critical point in the case of conversion reactions, which are interface driven and go through the continuous restructuring of the electrode material. The same is true for the alloying reaction, for which the electrochemical grinding produces a new exposed surface that might negatively interact with the electrolyte. A first attempt of using conversion materials was made using mixed Ni–Co oxide, which shows a reversible capacity close to 200 mAh g^{-1} versus Na.¹² Moreover, it is important to stress that the reaction of a specific material in the Na-ion cell is not expected to be trivially related to its behavior in a Li cell and that the reaction mechanism vs Na may in fact be different from the one observed vs Li.¹³ Indeed, a recent paper of Obrovac et al.¹⁴ demonstrated that the reaction mechanism of Sn with Na is different from the one with Li. In particular, these authors

Received: October 24, 2012

Published: November 29, 2012

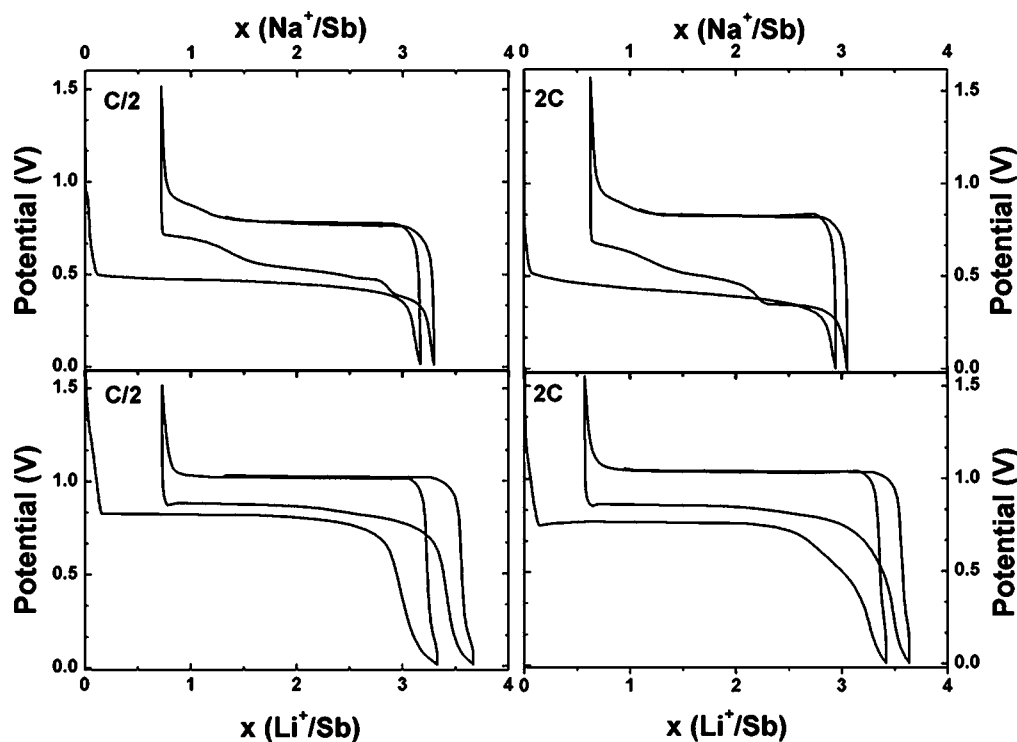


Figure 1. Composition–voltage profile for Sb/Na (top) and Sb/Li (bottom) cells cycled at C/2 and 2C rates between 1.5 and 0.02 V.

evidenced that the electrochemical alloying reaction may lead to specific instable phases that would not form through common chemical reaction paths.

Very recently, antimony-based nanocomposites have demonstrated interesting performances by sustaining reversible capacities between 500 and 600 mAh g⁻¹ over numerous cycles. The good performance obtained with mechanical milled Sb–C¹⁵ and SnSb–C¹⁶ composites has been attributed to the typical structural confinement occurring in these materials during the charge–discharge process.¹⁵ Differently from Sb–C nanocomposites, only very poor cycling performances (capacity lower than 100 mAh g⁻¹ only after 25 cycles) were reported for metallic Sb powders.¹⁵

In contrast to these poor performances, we show in this paper that even commercial micrometric Sb demonstrates outstanding cycling performances vs Na at a high rate, largely superior to the better known ones vs Li. A capacity of 600 mAh g⁻¹, very close to the theoretical one (610 mAh g⁻¹), is maintained over 160 cycles with a constant Coulombic efficiency exceeding 98%. The high crystallinity of the Sb material used in this study provides very well-defined electrochemical features, allowing the investigation of the electrochemical mechanism in situ by X-ray diffraction. The reaction mechanism with Na does not simply resemble the reversible alloying/dealloying mechanism observed in the case of lithium.

EXPERIMENTAL SECTION

The electrochemical performances of Sb (Alfa-Aesar 99.5% purity, ~325 mesh as negative electrode materials) were examined in two electrode Swagelok-type cells assembled in an argon-filled glovebox. Electrode formulation was made using a mixture of carbon black and vapor ground carbon fibers (VGCF-S) as the conductive additive and carboxymethyl cellulose (CMC) (DS = 0.7, *M_w* = 250 000 Aldrich) as the binder. The advantage of associating CMC and VGCF in electrode formulations was described elsewhere.^{17,18} An aqueous slurry

containing 70 wt % active material, 15 wt % binder, and 15 wt % conductive additive was homogeneously mixed by a planetary ball-milling for 1 h, tape casted on a 200 μm thick copper foil, and dried at room temperature for 12 h and finally at 100 °C under vacuum for another 2 h. The final mass loading of active material on the electrode was 1.4 mg cm⁻².

The electrochemical tests vs Na or Li were performed against a counter-electrode of the corresponding pure metal, using either 1 M NaClO₄ in PC or 1 M LiPF₆ in EC:PC:3DMC – 1% VC, with or without addition of 5% fluoroethylene carbonate (FEC), as the electrolyte, respectively. All tests were carried out at room temperature (25 °C).

In situ X-ray diffraction experiments were performed with an X'Pert diffractometer with Cu Kα radiation using a specifically developed electrochemical cell¹⁹ formed with a beryllium window as a current collector. The electrochemical measurements were controlled by a Mac pile system. The cell was cycled at a low rate of C/8 (reaction of one Na⁺ in 8 h), and the interval between X-ray patterns corresponds to 0.125 inserted or deinserted Na⁺.

RESULTS AND DISCUSSION

The voltage profiles at two different rates (C/2 and 2C, meaning 0.5 and 2 mole of Na or Li per mole of Sb per hour, respectively) of the first two cycles for Sb vs both Na and Li are shown in Figure 1. At the C/2 rate, the galvanostatic signature of Na is quite different from that of Li. For the latter, the first lithiation occurs on a single plateau at 0.81 V vs Li⁺/Li, and the following insertion/deinsertion cycles are also occurring following single plateaus at 0.85 and 1.05 V, respectively. The differences in shape and potential between the first insertion and the following ones are thus relatively small, indicating that in this case the reaction mechanism is most probably the same, as it has already been known for a long time.²⁰ At faster rates (2C), a similar profile is observed for Li, in spite of a slight increase in polarization which shifts the first plateau at 0.75 V. The following cycling reactions occur at almost the same potentials observed for cells cycled at the C/2 rate. It is

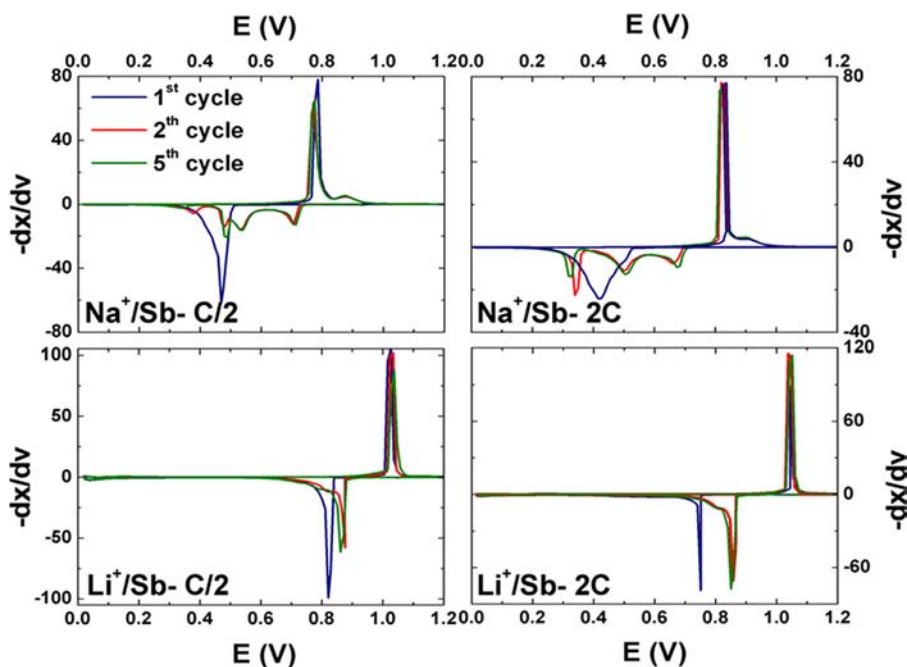


Figure 2. Derivatives of the composition–voltage profiles for Sb/Na and Sb/Li cells cycled at C/2 and 2C rates between 1.5 and 0.02 V.

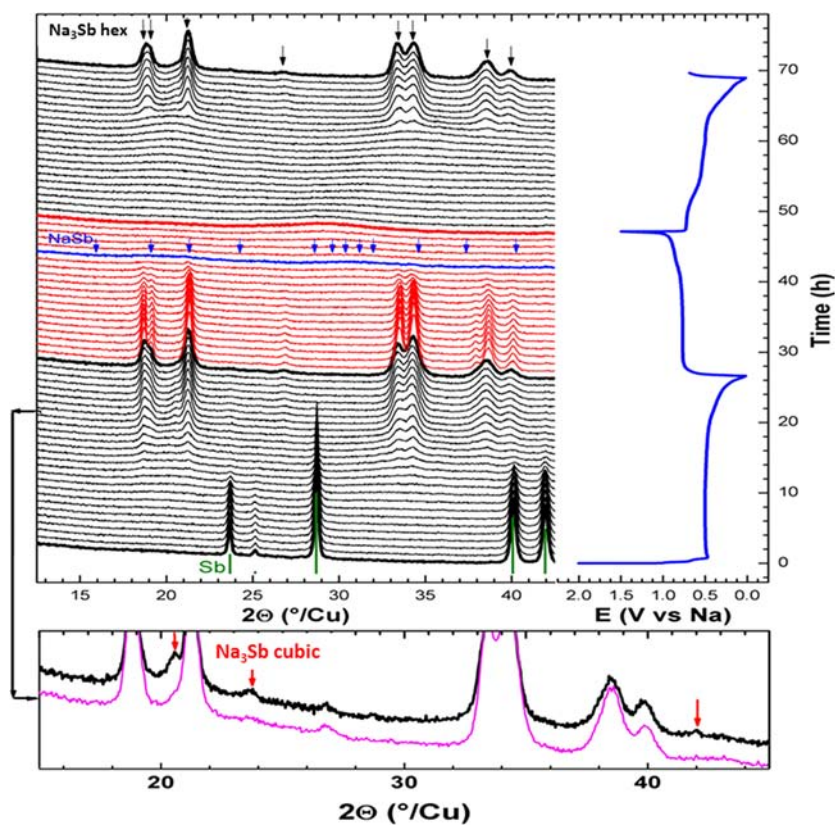


Figure 3. Operando evolution of the XRD pattern recorded at a C/8 rate (top left). The black and the red patterns are those recorded during the discharges and charge, respectively. The corresponding voltage profile (top right). A zoom illustrating the diffraction peaks from the cubic Na_3Sb (bottom).

important to notice that, regardless of the cycling rate, a slight tail is visible when the potential gets close to 0 V at the end of the first insertion, probably representing the decomposition of the electrolyte at the electrode surface according to the number of inserted Li ions compared to the theoretical value of 3

(corresponding to the formation of Li_3Sb , vide infra). This might also mean that the irreversible processes (decomposition of FEC, electrolyte, and insertion of cations into carbon) occur at different potentials for the two systems and perhaps have different reaction pathways.

The electrochemical curves of crystalline bulk Sb against Na interestingly provide rather different results. To our knowledge, this is the first time that such a well-defined galvanostatic signature of bulk Sb vs Na is reported. In fact, the work recently published by Qian et al.¹⁵ shows less-defined cycling curves due to the nanostructured nature of their starting Sb. Here the profile measured at $C/2$ shows a first insertion of Na occurring along a single long plateau at 0.45 V vs Na^+/Na , while the first deinsertion and the following ones show the presence of a first long plateau at 0.80 V and a much shorter one at 0.9 V. In the second insertion and in the following ones, however, three distinct plateaus are observed at 0.72, 0.55, and 0.50 V, as can be easily remarked in the derivative signal shown in Figure 2. This result is surprising since, differently from Li, it shows that the mechanism observed during the first discharge is different from that of the following ones. Moreover, only two different alloy compounds between Na and Sb are known in the Na–Sb phase diagram, i.e., NaSb and Na_3Sb .²¹ It is important to underline that the same features are observed during the following cycles and that, in particular, these three plateaus are perfectly reproducible. Finally, differently from the case of Li, no tail close to 0 V vs Na^+/Na is observed at the end of the first discharge, suggesting that at these working potentials the electrolyte is less sensitive to decomposition than in the case of Li.

At faster cycling rates, in addition to the expected increase in polarization between discharge and charge, an additional small plateau is observed only during the second discharge at 0.35 V. This plateau occurs at the same potential as for pristine Sb, suggesting the consumption of residual Sb that did not react completely during the first discharge (due to kinetic limitation). This plateau was barely visible already in the sample cycling at $C/2$ and vanishes upon further cycling. A very short solid solution region is observed at both regimes in the beginning of the first discharge (sloping region extending for 0.2 Na), which can be attributed to Na insertion in the carbon additive. Globally, the number of inserted ions is very close to the theoretical value of 3 corresponding to the formation of Na_3Sb in the case of sodium, whereas in the case of Li, a number of lithium ions slightly exceeding 3 is inserted, indicating that additional Li consumption occurs, most probably by parasite electrolyte decomposition reactions.

To better understand the reaction mechanism of Sb with Na, and in particular the unusual electrochemical features observed during discharge, the first two cycles were investigated by in situ XRD. At the beginning of the reaction, only the well-defined peaks of crystalline Sb are visible in the diffraction pattern (cf. Figure 3). During the first discharge, the intensities of these peaks decrease progressively without observing any new peak in the diffraction pattern until half discharge. Note that at this point of discharge in the Sb/Li battery the crystalline Li_2Sb phase is clearly appearing.²² It is only after the vanishing of Sb diffraction peaks, at about 1.7 reacted Na, that peaks corresponding to the hexagonal Na_3Sb (JCPDS No. 741162) start appearing.

An accurate observation of the diffraction patterns reveals a shoulder on the left of the peak at 20.5° . The magnified diagram (Figure 3, bottom) confirms that a new set of small peaks appears at 20.5 , 24 , and 42° . Those peaks are attributable to reflection from the cubic Na_3Sb . Leonova et al.²³ led a complete high-pressure study of Na_3Sb at room temperature and demonstrated that, even though the Na–Sb phase diagram (under atmospheric pressure) shows only one Na_3Sb

polymorph with a hexagonal crystal structure,²¹ the denser cubic phase can be stabilized at room temperature in the pressure range between 10^{-4} and 9.0 GPa. It is noteworthy that the formation of “high-pressure” phases has already been observed in the cycling of antimonides vs Li, showing the high metastability of the intermediate phases formed during the lithiation/delithiation of intermetallic phases,²⁴ and is in line with similar results presented by Obrovac et al. for the Na–Sn system.¹⁴

The in situ pattern at key steps of the first two cycles is given in Figure 4a. While the hexagonal Na_3Sb phases formed at the

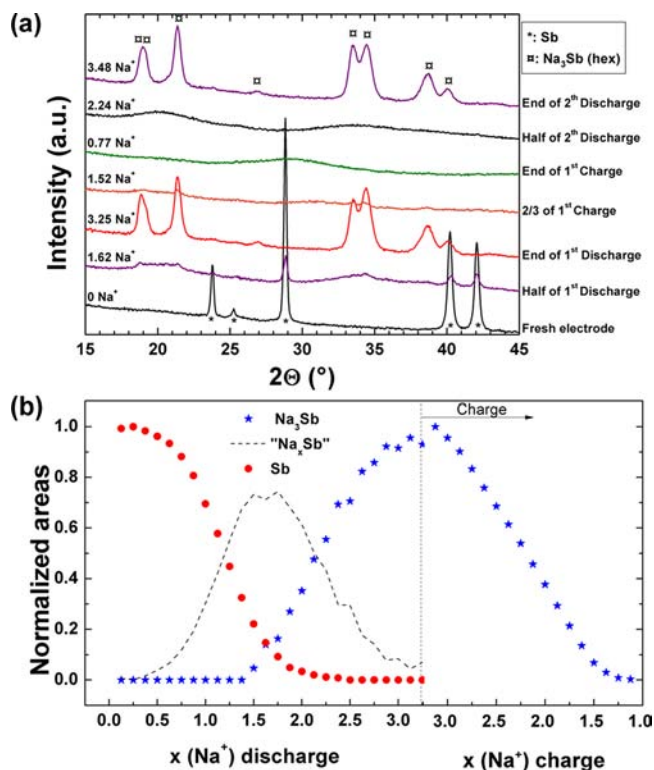


Figure 4. (a) Selected operando XRD patterns at various stages of discharge and charge of a Sb/Na cell. *, and □ were used to indicate the Bragg peaks corresponding to Sb and Na_3Sb , respectively. (b) Normalized areas under the most intense diffraction peaks for Sb (28.8°) (in red) and Na_3Sb (21.2°) (in blue) during the first cycle plotted as a function of reacted sodium ions (x). The dashed line represents the calculated intensity of amorphous Na_xSb phase.

end of the first and second discharge show a remarkable crystallinity (for an electrochemically structured phase), the phase obtained at the end of the charge is completely amorphous. However, one can distinguish a very broad peak centered at 29° that can be attributed to amorphous Sb. To get a clear view of the chronology of phase evolution during cycling, the intensity of the peak at 28.8° of Sb (in red) and of that of hexagonal Na_3Sb at 21.2° (in blue) for the first cycle are plotted as a function of reacted sodium ions (x). The fact that Na_3Sb starts to appear only after the vanishing of the diffraction peaks of Sb implies the formation of a completely amorphous intermediate phase. The evolution of the amount of this amorphous phase can be estimated by subtracting the normalized area of Sb and Na_3Sb from unity as shown by the dashed line in Figure 4 (bottom). The amorphous phase reaches its maximum at a composition (Na_xSb with $x \sim 1.5$) close to the expected NaSb from the phase diagram. In

summary, these observations clearly indicate that Sb first transforms upon discharge into an intermediate amorphous phase Na_xSb , not detectable by XRD, and only when all the Sb has almost completely reacted this Na_xSb amorphous phase starts converting into cubic-hexagonal Na_3Sb mixture phases before being stabilized as hexagonal Na_3Sb . It is important to notice that both transformations occur at virtually the same potential.

During charge, the profiles of Na_3Sb gradually disappear, leading to an almost flat diffractogram at about two extracted Na. From this flat diffractogram, a very broad peak in correspondence to the main reflection of Sb metal appears around 29° , probably indicating the formation of amorphous Sb. The appearance of the completely flat diffractogram matches the reversible reaction of about 1.5 Na, which corresponds to a completely amorphous Na_xSb phase. The following second discharge thus starts from completely amorphous Sb metal, which transforms first into an amorphous compound giving very broad diffraction profiles at angles corresponding to the most intense reflections of hexagonal/cubic Na_3Sb . The intermediate Na_xSb phase transforms back to Na_3Sb . The following subsequent cycles show the same mechanism as first charge and second discharge, indicating that a very reversible mechanism takes place between two phases going through (at least) one amorphous intermediate compound.

It is interesting to note that electrochemical reactions occurring in a Li/Sb cell were previously determined^{22,25} and are consistent with the sequential formation of crystallized Li_2Sb (Li_2Sb space group $P62c$, Hexagonal, $a = 7.918 \text{ \AA}$ and $c = 3.242 \text{ \AA}$) and crystallized Li_3Sb (Li_3Sb , space group $Fm\bar{3}m$, no. 225, cell parameter $a = 6.572 \text{ \AA}$, $V = 283.9 \text{ \AA}^3$).²⁶ Note that the face-centered-cubic Li_3Sb polymorph, which is formed during the lithiation of Sb as well as during the lithiation of all antimonides reported in the literature, is designated in the Li/Sb phase diagram as the high-temperature polymorph (the ambient temperature $\alpha\text{-Li}_3\text{Sb}$ transforms to $\beta\text{-Li}_3\text{Sb}$ at temperatures above $650 \text{ }^\circ\text{C}$).^{24,27–29} On the electrochemical curve of the Sb/Li cell (Figure 1a), only one potential plateau (or derivative peak) characterizes the two phase transitions Sb into Li_2Sb and Li_2Sb into Li_3Sb . The behavior of Li/Sb during charge is very different. No evidence of Li_2Sb is observed during any part of the charge cycle, and instead, Li_3Sb converts directly back to crystalline Sb as Li is removed. Li_2Sb peaks reappear during the second discharge.

Table 1 summarizes the main phase reactions in Sb/Li and Na/Li cells. While an intermediate crystalline phase, namely,

Table 1. Electrochemical Reactions in the Sb/Li vs Sb/Na Cells

	Na	Li
discharge	$\text{Sb} \rightarrow \text{Na}_x\text{Sb}$ $\text{Na}_x\text{Sb} \rightarrow \text{Na}_3\text{Sb}_{\text{hex}}/\text{Na}_3\text{Sb}_{\text{cub}} \rightarrow \text{Na}_3\text{Sb}_{\text{hex}}$	$\text{Sb} \rightarrow \text{Li}_2\text{Sb}$ $\text{Li}_2\text{Sb} \rightarrow \text{Li}_3\text{Sb}$
charge	$\text{Na}_3\text{Sb}_{\text{hex}} \rightarrow \text{Sb}$	$\text{Li}_3\text{Sb} \rightarrow \text{Sb}$

c: crystalline. a: amorphous.

Li_2Sb , is identified by XRD upon discharge before the formation for Li_3Sb in the Li/Sb cell, no crystalline intermediate phase could be detected by XRD for the Na/Sb cell, neither on discharge nor on charge.

The different behavior of the Na/Sb and Li/Sb systems may have to do with the differing structures of Na_3Sb (the hexagonal

phase is stabilized at the end of discharge) and low-temperature Li_3Sb rock salt structure.

The most surprising and interesting consequences of this cycling mechanism are however the outstanding performances of Sb vs Na compared to those usually observed with Li, which are summarized in Figure 5. It is important to underline that

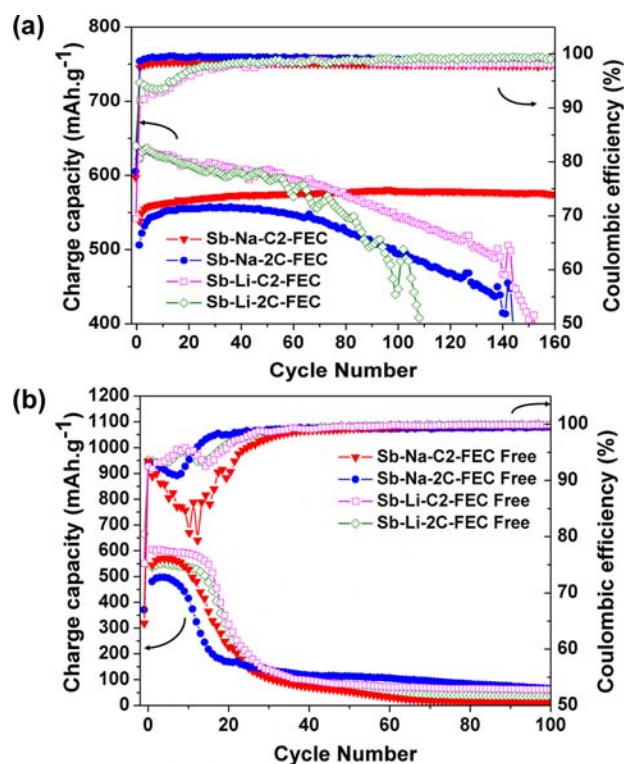


Figure 5. (a) Cycling performance of Sb electrode vs Na^+ and Li^+ at C/2 and 2C with (top) and (b) without (bottom) addition of 5% FEC.

electrodes prepared in exactly the same way (cf. Experimental Section) were used for both Li and Na experiments and that the results shown here are perfectly reproducible. Electrolytes both containing and without FEC were used for parallel tests: FEC was shown to improve the cycling performances of both Na and Li independently of the cycling rate, the capacity collapsing after about 15 cycles when this additive is not added to the electrolyte (see Table 2). When FEC is used, however, remarkable differences in cycling performances between Na and Li are observed. In the case of Li, the capacity initially exceeds slightly the theoretical value but then decays slowly upon cycling. A relatively low Coulombic efficiency (after the first cycle) of about 90% is observed during the first 15 cycles, which confirms that some lithium is consumed by decomposition side reactions with the electrolyte. In the case of Na, on the contrary, an outstanding good cycling life of the Sb electrode is observed at C/2, with a stable capacity of 576 mAh g^{-1} after 160 cycles and a surprisingly good Coulombic efficiency (after the first cycle) exceeding 98%. At higher rates, the performances of Sb vs Na still remain good (525 mAh g^{-1} after 50 cycles), showing an even superior Coulombic efficiency.

Figure 6 shows the rate cycling behavior of the Sb/Na electrode. The cell delivers a charge capacity of $609\text{--}528 \text{ mAh g}^{-1}$ at sequential charge rates of C/10 to 4C rates, respectively. When the rate is reset to C/10 after 65 cycles, the capacity is

Table 2. Charge Capacity (mAh g^{-1}) of Sb/ Na^+ and Sb/ Li^+ Electrodes at C/2, 2C, and 4C Rates

cycle number	Sb/ Na^+ electrode						Sb/ Li^+ electrode						
	FEC			FEC-Free			FEC			FEC-Free			
	1st	80th	C. E. ^a (%)	1st	80th	C. E. (%)	1st	80th	C. E. (%)	1st	80th	C. E. (%)	
rates	C/2	537	576	98	544	14	98	622	573	98	604	66	99
	2C	506	524	99	480	84	99	623	544	99	536	38	99
	4C	491	372	99	-	-	-	523	360	99	-	-	-

^aCoulombic efficiency (%).

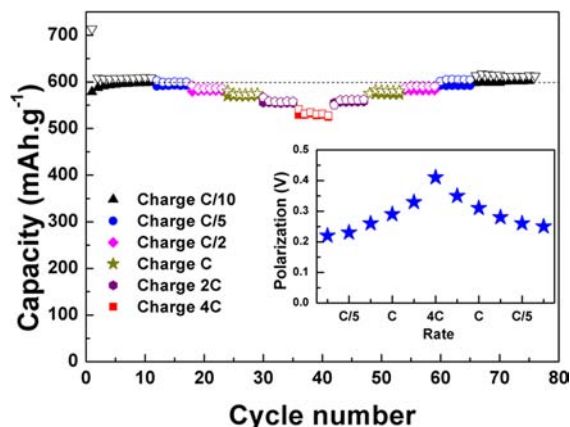


Figure 6. Rate capability (and polarization, inset) of the Sb/Na electrode at various current rates from C/10 to 4C. Open and filled symbols are for discharge and charge, respectively.

recovered and is even slightly ahead of the capacity measured in the first set at C/10, which indicates good tolerance for the rapid Na ion insertion/extraction. The rate capabilities are summarized in Table 2 with the capacity values measured at C/2, 2C, at 4C rates for the 1st and 80th cycles of Sb/Li and Sb/Na systems. The delivered capacity at 4C is 16% lower than that obtained at C/2 for lithium but only 8% for Na. These results clearly indicate that the Sb/Li system is more kinetically limited than the Sb/Na one. However, one can observe that the polarization of the cycle (inset of Figure 6) reversibly increases with the cycling regime, showing that kinetics remain a limitation for the Sb/Na cells.

The irreversible capacity at the first cycle (cf. Figure 1), which should correspond to the formation of a Solid Electrolyte Interphase (SEI) layer on the Sb electrode and on the carbon additive, is very similar for both Li and Na.

This irreversible consumption is lower when the electrolyte contains FEC than in the case of FEC-free electrolytes and apparently leads to the formation of a stable and thus beneficial SEI layer, as testified by the very good Coulombic efficiency. Note that the Coulombic inefficiencies observed in early cycles of Na/Sb cells and Li/Sb partially due to the irreversible insertion of alkali metal ions into the carbon black conductive additive could probably be reduced by the optimization of the electrode formulation and structuration.

The low potential tail at the end of the discharge observed in the case of Li and completely absent in the case of Na indicates that some electrolyte decomposition occurs at low potentials in Li cells at least during the first 15 cycles, explaining the superior performances of the Na ones. It should be underlined that FEC is known to promote longer cycle lives in silicon-based electrodes,^{30,31} in conversion materials,³² and also in the case of sodium batteries utilizing both Sb/C¹⁶ and hard carbon

anodes.³³ Our results extend this list and confirm that FEC is a very beneficial electrolyte additive for electrodes working at low potential and, above all, that Na profits from the protection of FEC to a much larger extent than Li.

Finally, it must be noticed that our results partly contradict those obtained by Qian et al.,¹⁵ who also studied bulk Sb as a reference compound, obtaining much inferior performances, however. Differently from their nanostructured Sb composite obtained through expensive milling treatments and contrary to common knowledge, a simpler Sb-based electrode more easily and cheaply prepared using raw commercial micrometric Sb without any pretreatment leads to outstanding cycling performances at high rates. In our case, the use of a different and more efficient carbon additive containing carbon fibers^{17,18} coupled to slightly larger amounts of CMC binder might be a first explanation of these strongly improved performances.

CONCLUSION

In agreement with a recent review paper related to layered compounds,¹³ we show through the present comparative study of Sb vs both Na and Li that the reaction behavior of a material with Na is not simply and straightforwardly related to its performances in Li cells but that a different chemistry takes place while reacting with Na. In the case of Sb, the reaction vs Li goes through an alloying/dealloying process, whereas the process in Na/Sb is not fully elucidated but appears to be more complex than that for the Li/Sb system since amorphous intermediate phases are observed for the former but not for the latter during the cycling. While in the case of Li the intermediate species usually formed upon cycling are those expected from the phase diagram, in the case of Na the intermediate phases are mostly amorphous and could not be precisely identified. Moreover, we evidenced that a competition takes place at the end of the discharge of the Sb/Na cell between the formation of the hexagonal and the cubic polymorphs of Na_3Sb , the last being described in the literature as unstable at atmospheric pressure. In addition to the positive effect of the electrode engineering and the use of a SEI forming additive (FEC), the good cycling of the Na/Sb system compared to the Li/Sb system and previous intermetallic/Li systems is indeed a striking result. This might be partially due to decreased volume expansion upon going from Sb (181.1 \AA^3) to hexagonal Na_3Sb (237 \AA^3) compared to rock salt Li_3Sb (283.8 \AA^3). Moreover, the intermediate amorphous phase seen in the case of Na insertion may act as a buffer to relieve strain, accounting for the improved cycling seen in the system.

The outstanding properties of Sb vs Na are completely unexpected and can form the basis for the development of new negative electrode chemistry for Na-ion batteries which could be considered as not viable in the case of the Li-ion ones. As a consequence, conversion and/or intermetallic phases that were already studied in the case of Li-ion batteries might be possible

candidates for Na-ion batteries provided that they present a working potential exceeding that of the redox couple Na^+/Na . All conversion-type materials thus become potentially interesting anode materials for Na-ion batteries and need to be urgently revisited; outstanding electrochemical performances could be achievable.

AUTHOR INFORMATION

Corresponding Author

laure.monconduit@univ-montp2.fr

Author Contributions

All authors contributed equally to this work.

Notes

The authors declare no competing financial interest.

ACKNOWLEDGMENTS

This research was performed in the framework of ALISTORE-ERI. The authors are indebted to Henry Wilhelm and Bernard Lestriez for their helpful advice on formulation.

REFERENCES

- (1) Tarascon, J.-M. *Nature Chem.* **2010**, *2*, 510.
- (2) Kawamoto, H.; Tamaki, W. *Sci. Technol. Trends, Quart. Rev.* **2011**, *39*, 51.
- (3) Delmas, C.; Fouassier, C.; Hagenmuller, P. *Phys. B+C* **1980**, *99*, 81.
- (4) Cao, Y.; Xiao, L.; Wang, W.; Choi, D.; Nie, Z.; Yu, J.; Saraf, L. V.; Yang, Z.; Liu, J. *Adv. Mater.* **2011**, *23*, 3155.
- (5) Senguttuvan, P.; Rousse, G.; Seznec, V.; Tarascon, J.-M.; Palacin, M. R. *Chem. Mater.* **2011**, *23*, 4109.
- (6) Komaba, S.; Nakayama, T.; Ogata, A.; Shimizu, T.; Takei, C.; Takada, S.; Hokura, A.; Nakai, I. *ECS Trans.* **2009**, *16*, 43.
- (7) Alcántara, R.; Lavela, P.; Ortiz, G. F.; Tirado, J. L. *Electrochem. Solid-State Lett.* **2005**, *8*, A222.
- (8) Doeff, M. M.; Ma, Y.; Visco, S. J.; De Jonghe, L. C. *J. Electrochem. Soc.* **1993**, *140*, L169.
- (9) Komaba, S.; Murata, W.; Ishikawa, T.; Yabuuchi, N.; Ozeki, T.; Nakayama, T.; Ogata, A.; Gotoh, K.; Fujiwara, K. *Adv. Funct. Mater.* **2011**, *21*, 3859.
- (10) Ong, S. P.; Chevrier, V. L.; Hautier, G.; Jain, A.; Moore, C.; Kim, S.; Ma, X.; Ceder, G. *Energy Environ. Sci.* **2011**, *4*, 3680.
- (11) Cabana, J.; Monconduit, L.; Larcher, D.; Palacin, M. R. *Adv. Mater.* **2010**, *22*, E170.
- (12) Alcántara, R.; Jaraba, M.; Lavela, P.; Tirado, J. L. *Chem. Mater.* **2002**, *14*, 2847.
- (13) Kim, S.-W.; Seo, D.-H.; Ma, X.; Ceder, G.; Kang, K. *Adv. Energy Mater.* **2012**, *2*, 710.
- (14) Ellis, L. D.; Hatchard, T. D.; Obrovac, M. N. *J. Electrochem. Soc.* **2012**, *159*, A1801.
- (15) Qian, J.; Chen, Y.; Wu, L.; Cao, Y.; Ai, X.; Yang, H. *Chem. Commun.* **2012**, *48*, 7070.
- (16) Xiao, L.; Cao, Y.; Xiao, J.; Wang, W.; Kovarik, L.; Nie, Z.; Liu, J. *Chem. Commun.* **2012**, *48*, 3321.
- (17) Lestriez, B.; Desaevers, S.; Danet, J.; Moreau, P.; Plée, D.; Guyomard, D. *Electrochem. Solid-State Lett.* **2009**, *12*, A76.
- (18) Sivasankaran, V.; Marino, C.; Chamas, M.; Soudan, P.; Guyomard, D.; Jumas, J.-C.; Lippens, P.-E.; Monconduit, L.; Lestriez, B. *J. Mater. Chem.* **2011**, *21*, 5076.
- (19) Leriche, J. B.; Hamelet, S.; Shu, J.; Morcrette, M.; Masquelier, C.; Ouvrard, G.; Zerrouki, M.; Soudan, P.; Belin, S.; Elkaim, E.; Baudalet, F. *J. Electrochem. Soc.* **2010**, *157*, A606.
- (20) Weppner, W.; Huggins, R. A. *J. Electrochem. Soc.* **1978**, *125*, 7.
- (21) Songster, J.; Pelton, A. D. *J. Phase Equilib.* **1993**, *14*, 250.
- (22) Hewitt, K. C.; Beaulieu, L. Y.; Dahn, J. R. *J. Electrochem. Soc.* **2001**, *148*, A402.
- (23) Leonova, M. E.; Bdiqin, I. K.; Kulinich, S. A.; Gulish, O. K.; Sevast'yanova, L. G.; Burdina, K. P. *Inorg. Mater.* **2003**, *39*, 332.
- (24) Villevieille, C.; Ionica-Bousquet, C.-M.; Ducourant, B.; Jumas, J.-C.; Monconduit, L. *J. Power Sources* **2007**, *172*, 388.
- (25) Wang, J.; Raistrick, I. D.; Huggins, R. A. *J. Electrochem. Soc.* **1986**, *133*, 457.
- (26) Brauer, G.; Zintl, E. *Z. Phys. Chem.* **1937**, *B37*, 323.
- (27) Fransson, L. M. L.; Vaughey, J. T.; Benedek, R.; Edström, K.; Thomas, J. O.; Thackeray, M. M. *Electrochem. Commun.* **2001**, *3*, 317.
- (28) Morcrette, M.; Larcher, D.; Tarascon, J. M.; Edström, K.; Vaughey, J. T.; Thackeray, M. M. *Electrochim. Acta* **2007**, *52*, 5339.
- (29) Villevieille, C.; Fraise, B.; Womes, M.; Jumas, J.-C.; Monconduit, L. *J. Power Sources* **2009**, *189*, 324.
- (30) Etacheri, V.; Haik, O.; Goffer, Y.; Roberts, G. A.; Stefan, I. C.; Fasching, R.; Aurbach, D. *Langmuir* **2012**, *28*, 965.
- (31) Lin, Y.-M.; Klavetter, K. C.; Abel, P. R.; Davy, N. C.; Snider, J. L.; Heller, A.; Mullins, C. B. *Chem. Commun.* **2012**, *48*, 7268.
- (32) Wilhelm, H.; Darwiche, A.; Marino, C.; Monconduit, L.; Lestriez, B. *Electrochem. Commun.* **2012**, *24*, 89–92.
- (33) Komaba, S.; Ishikawa, T.; Yabuuchi, N.; Murata, W.; Ito, A.; Ohsawa, Y. *ACS Appl. Mater. Interfaces* **2011**, *3*, 4165.